Self-Assembly of Heterogeneous Supramolecular Structures with Uniaxial Anisotropy

ARTICLE *in* THE JOURNAL OF PHYSICAL CHEMISTRY B · JANUARY 2007

Impact Factor: 3.3 · DOI: 10.1021/jp066493x · Source: PubMed

THE JOURNAL OF PHYSICAL CHEMISTRY B LETTERS

2006, *110,* 25573−25577
Published on Web 12/07/2006

Self-Assembly of Heterogeneous Supramolecular Structures with Uniaxial Anisotropy

M. Ruiz-Osés,[†] N. González-Lakunza,[‡] I. Silanes,[§] A. Gourdon,[⊥] A. Arnau,[‡,#] and J. E. Ortega*[,†,#]

Departamento de Física Aplicada I, Universidad del País Vasco, Plaza de Oñate 2, E-20018 Donostia-San Sebastián, Spain, Departamento de Física de Materiales UPV/EHU, Facultad de Química, Apartado 1072, San Sebastian E-20080, Spain, Kimika Fakultatea, Euskal Herriko Unibertsitatea, P.K. 1072, 20080 Donostia, Euskadi, Spain, Groupe NanoSciences, CEMES-CNRS (UPR 8011), BP 94347, 29 Rue J. Marvig, 31055 Toulouse Cedex 4, France, and Unidad de Física de Materiales, Centro Mixto CSIC-UPV/EHU, Manuel Lardizabal 3, E-20018 San Sebastián, Spain

Received: October 3, 2006; In Final Form: November 21, 2006

Uniaxial anisotropy in two-dimensional self-assembled supramolecular structures is achieved by the coadsorption of two different linear molecules with complementary amine and imide functionalization. The two-dimensional monolayer is defined by a one-dimensional stack of binary chains, which can be forced to line up along steps in vicinal surfaces. The competing driving forces in the self-organization process are discussed in light of the structures observed during single molecule adsorption and coadsorption on flat and vicinal surfaces and the corresponding theoretical calculations.

Molecular recognition, that is, selective molecular interaction, is at the basis of fundamental biological processes in living systems, ranging from DNA replication or virus attachment to cells, to a number of nanotechnology applications that mimic these phenomena, such as nanoparticle surface functionalization for molecule or cell targets. Molecular recognition is also the driving force in the supramolecular self-assembly of organic molecular multilayers used in nanoelectronic devices.[1] Both supramolecular chemistry and molecular recognition strategies can be jointly exploited in the fabrication of nanostructured templates for molecule adsorption on surfaces. For such purposes, planar ring systems (polyarenes) are very suitable, particularly with noble metals as substrates, since they adsorb flat and diffuse quickly on the surface plane. In particular, stable supramolecular structures can be obtained by coadsorbing two molecules with complementary end-groups, such as pairs of DNA bases.[2] Synthetic chemistry allows one to tune the lattice parameter, by varying the size of the polyarenes, and the symmetry, by inserting functional groups in the appropriate geometry. One good example is the coadsorption of diaminotriazine (melamine) and perylene tetracarboxylic diimide (PTCDI),[3,4] which leads to a supramolecular (H-bonded) honeycomb network driven by both the strong PTCDI−melamine (imide/amine) affinity and the threefold symmetry of the melamine. Here we show that, by selecting a pair of chemically complementary polyarenes with linear shape and imide/amine end-groups, one obtains the one-dimensional (1D) heterogeneous molecular network analogue, that is, a 1D binary chain with strong intermolecular H-bonding.

Functional structures made of molecular recognition patterns require well-defined arrays at higher hierarchical levels. Here, the substrate plays the key role. Homogeneous patterns spanning large surface areas are effectively limited by terrace morphologies and substrate reconstruction domains.[5] Mesoscopic ordering can be achieved by self-assembled prepatterned surfaces, such as vicinal surfaces, that is, 1D arrays of monatomic steps.[6] The latter not only introduce the uniaxial anisotropy in the system, but also can induce single domains in the mesoscopic scale.[7] As we show in this work, one can combine vicinal substrates and a pair of linearly shaped molecules with complementary (imide/amine) end-groups to achieve self-organized supramolecular assemblies with a well-defined uniaxial anisotropy with respect to a surface direction, namely, the step direction.

In order to test this prepatterning-plus-self-assembly approach of binary structures, we use benzodiguanamine (BDG) ($C_{12}H_{12}N_{10}$), which is a linear version of melanine, and naphtalene tetracarboxylic diimide (NTCDI) (C_{14} $H_8N_2O_4$), which is similar to PTCDI, as well as a Au(111) vicinal surface with periodic faceting. The atomic structures of these two molecules are schematically shown in Figure 1. The complementary functionalization is expected to favor the formation of dimers with strong triple H-bonds, as depicted in the figure. BDG is synthesized by the reaction of dicyandiamide with terephthalonitrile in EGME/potassium hydroxide under microwave irradiation. The product of the reaction that we call BDG is 1,4-di(4,6-diamino-1,3,5-triazin-2-yl)benzene. On flat surfaces, a two-dimensional (2D), binary supramolecular structure is readily achieved, which is formed by packing 1D heterogeneous NTCDI/BDG rows. Theoretical calculations fit structural observations and demonstrate that the triple H-bond in the frontal

* Corresponding author.
[†] Universidad del País Vasco.
[‡] Facultad de Química.
[§] Euskal Herriko Unibertsitatea.
[⊥] CEMES-CNRS (UPR 8011).
[#] Centro Mixto CSIC-UPV/EHU.

10.1021/jp066493x CCC: $33.50

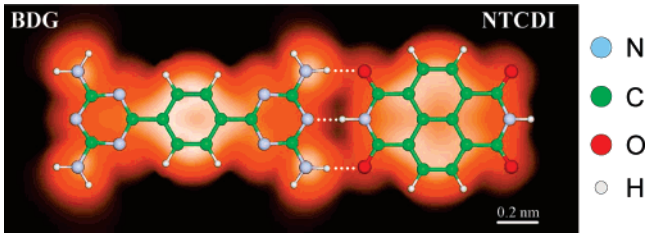

Figure 1. BDG and NTCDI molecule structures. The respective amine and imide terminations favor the formation of dimers with strong triple H-bonding. The schematic atomic arrangement is superimposed on a calculated STM image for a BDG−NTCDI dimer on Au(111) (see the text).

interaction (∼14.4 kcal/mol) shown in Figure 1 is much stronger than the lateral binding energy between adjacent dimers, (∼4.6 kcal/mol), thereby defining a highly anisotropic supramolecular assembly. Such uniaxial anisotropy is indeed forced along the step edge direction using the vicinal Au surface. However, we find that the sharply defined, binary NTCDI/BDG array only exists inside relatively wide terraces, coexisting with other phases with different stoichiometry, namely, BDG-rich mixtures decorating step edges and pure NTCDI arrays filling terraces. Such behavior is understood from the different tendency to aggregate on terraces (NTCDI) or stick to surface steps (BDG).

The experiments were performed in an ultrahigh vacuum system (base pressure below 5×10^{-11} mbar) equipped with a commercial Omicron scanning tunneling microscope (STM) that operates at 300 K. BDG and NTCDI were evaporated from efussion cells. The mixture was additionally annealed to ∼450 K (right below the desorption temperature for BDG) in order to improve the layer crystallinity. Pure NTCDI and BDG and mixed NTCDI + BDG 1 mL phases were first studied on Au(111) and then on Au(455). The latter is vicinal to Au(111) with a tilt angle of ∼5.7° toward the [11$\bar{2}$] direction. The clean Au(455) surface displays a quasi-periodic, faceted structure made of large (>100 nm), alternating Au(233) and Au(677) phases, which are, in turn, defined by periodic arrays of ∼14 and ∼32 Å wide terraces, respectively.[8] All surfaces were prepared by standard sputter−annealing cycles. Theoretical calculations were carried out to elucidate the gas-phase geometry of tetramer structures of these molecules using Gaussian 98[9] and Gaussian 03[10] to perform the optimizations at the B3LYP/6-31G level. The simulation of STM images shown in Figure 1 was performed in the Tersoff−Hamann approximation[11] using first-principle density functional theory (DFT) calculations. We used the Vienna Ab-inition Simulation Package (VASP)[12] within the Projector Augmented Wave method[13] to treat electron−ion interactions and the Generalized Gradient Approximation for exchange and correlation.[14] In these calculations, we used a periodic super-cell approach in which a four-layer Au(111) slab as well as the planar molecule are used. As weak dispersive forces between the molecule and the Au(111) surface cannot be described within DFT, we checked that the appearance of STM images does not change in a physically acceptable molecule−surface distance range of around 3 Å.[15] Since we neglect the interaction with the Au substrate and the eventual deviations from the planar geometry, and noting that DFT-GGA calculations are at the limit to describe H-bonds, we expect some discrepancy between calculated and measured lattice constants.

The images of Figure 2 a,b show characteristic STM topographies for self-assembled monolayer structures of pure BDG and NTCDI, respectively. We selected special tunneling conditions to enhance the detection of HOMO orbitals in both cases. We observe flat monolayer islands with a smooth undulation related to the herringbone reconstruction of the Au(111) underneath. However, a residual molecule/substrate interaction remains, since the periodicity of the herring bone is larger along the [1$\bar{1}$0] direction in both BDG (by 23%) and NTCDI (by 9%) layers with respect to the uncovered surface. Scanlines taken across the different symmetry directions on the STM image permit one to extract the oblique lattice parameters. These are 11.0 × 10.8 Å (with $\theta = 80.8°$, as marked in the lower panels of Figure 2) for NTCDI, and 13.4 × 11.4 Å ($\theta = 47.3°$) for BDG. The structures shown below Figure 2a,b have been calculated for the respective relaxed tetramers obtained from gas-phase calculations.

For NTCDI, the minimum energy structure corresponds to the α phase shown in the bottom panel of Figure 2b, which is defined by a 10.3 × 9.4 Å ($\theta = 72.9°$) lattice, that is, shorter than the measured unit cell. Since the observed structure exhibits registry with the Au fcc lattice underneath, such disagreement may be explained by the interaction with the substrate.[16] Nonetheless, the individual molecule orientation on the surface plane cannot be determined in the present STM image. Thus a

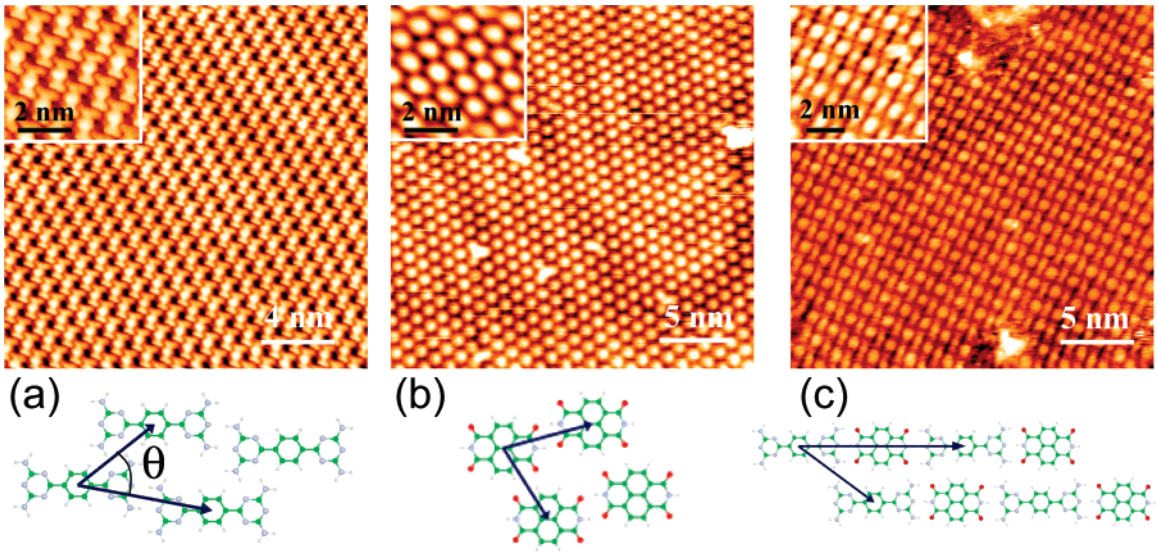

Figure 2. STM topographies showing monolayer-thick structures of (a) BDG (−0.27 V, 0.045 nA), (b) NTCDI (−1.6 V, 0.162 nA), and (c) NTCDI−BDG (−0.6 V, 0.103 nA) on Au(111). In the corresponding bottom panels, theoretically calculated tetramer structures are shown, with the corresponding 2D lattice vectors.

packed structure with alternatively tilted molecules along the short axis (γ phase), such as the one proposed by Keeling et al. for NTCDI on Ag/Si(111),[17] is also possible. For the α phase, the NH···O bond length is 1.8 Å, and the CH···O bond length is 2.18 Å. For BDG, the stable phase is the one shown in the inset, with lattice parameters 14.39 × 10.31 Å (θ = 49.0°). Thus, short and long axes are respectively expanded and contracted with respect to the experiment. The interaction with the substrate again explains such differences. One can indeed observe that the BDG monolayer is in perfect registry with the herring bone superlattice.[16] For the molecule arrangement shown in the bottom panel of Figure 2a, the corresponding HNH N bond lengths are 2.02 and 2.13 Å for the frontal and lateral bonds, respectively, that is, there is a relatively strong, complementary HNH···N doublet along the molecule axis and a weaker sideways bonding. The latter is defined by the interaction of the proton of the remaining NH_2 group with the inner N atom of the triazene.

The image in Figure 2c shows the monolayer structure after the coevaporation of 1 mL of NTCDI and BDG on Au(111). Self-assembly and mutual molecular recognition steer the system to a packed structure (26.0 × 13.7 Å, θ = 35.6°) with alternating BDG−NTCDI dimers. A modified substrate reconstruction is barely observable under the molecule layer, although binary chains are not aligned along high-symmetry directions of the Au crystal. The shape of the molecular features seen in the STM images is nicely reproduced by our STM simulations shown in Figure 1. The latter allows us to identify the relative orientation of the more rounded NTCDI molecule within the assembly. The optimized calculated tetramer structure (24.3 × 15.4 Å, θ = 34.03°) is shown in the bottom panel of Figure 2c. It matches reasonably well the relative orientation and lattice constant obtained in the STM image. Thus, molecule/substrate interactions do not appear to influence the equilibrium heterocomplex structure. The frontal NH···N and NH···O bond distances are 1.63 and 1.71 Å, respectively, whereas the lateral HNH···O bond is 3.07 Å long. Such a difference reflects a weaker hydrogen bond between the 1D chains, as compared to the stronger BDG/NTCDI bonding along chains. We must also note that defects in the binary structures have been observed, although these are mostly limited to stacking fault lines parallel to the 1D chains. Point defects along the chains appear very seldom. Therefore, the NTCDI/BDG monolayer can be thought of as a 1D stack of alternating, heterogeneous NTCDI/BDG wires.[18]

Figure 3 shows STM images after the coevaporation of ~0.9 mL of 50% NTCDI and 50% BDG on Au(455). Well-oriented binary structures are indeed obtained over large portions of the surface, but coexist with pure-NTCDI and BDG-rich areas. The different phases are marked as I, II, III, and IV in the upper panel of Figure 3. In the absence of substrate defects (such as the one shown in the left lower corner), the different phases extend a few microns in the direction parallel to the steps with a reduced width in the perpendicular direction. Thus, phase boundaries are located at step edges (blue dotted lines), and hence an effectively 1D phase separation operates. The substrate actually keeps its periodic faceting underneath, with the two different terrace sizes.[19] The wide-terrace facets contain phase I (binary), phase II (NTCDI), and phase III (BDG-rich), whereas the narrow-terrace facet hosts only the BDG-rich phase IV. The binary phase I, namely, the heterogeneous molecular recognition structure, is shown in the central panel. It is analogous to the one obtained on Au(111) shown in Figure 2b, but the vicinal surface allows us to obtain a single domain lined up with the step array. We see a 9% compression along NTCDI/BDG chains

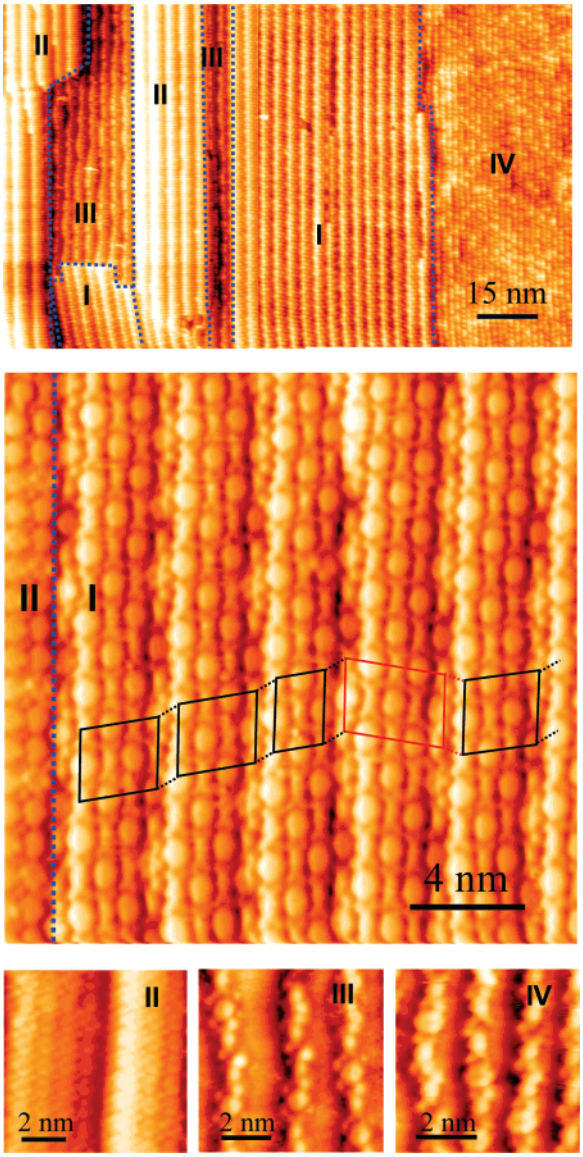

Figure 3. Top, coadsorption of 0.9 mL of NTCDI and BDG on Au(455). A 1D, multiple phase separation (dotted blue lines) is observed. The binary, single domain molecular recognition structure lined up along step edges (phase I) is shown in the central panel. Black rhomboids mark the regular packing sequence of 1D chains on terraces, which is reversed in one of them (red rhomboid). The bottom panels show the detailed view of phases II (NTCDI), III (BDG-rich on wide terraces), and IV (BDG-rich on narrow terraces).

with respect to the calculated structure, which could be due to the anchoring of the molecules at step edges, although such interaction remains unclear. Phase I is defined by a compact binary structure, namely, a regular packing of four 1D NTCDI/BDG wires per terrace (black rhomboids), with a different packing sequence across step edges (dotted lines). We note the presence of terraces with a reversed packing (red rhomboids), which are accompanied by stacking fault lines at the contiguous lower and upper steps. We can thus conclude that a residual interaction between rows in contiguous terraces exists, in contrast to a stronger row-to-row interaction inside terraces.

A closer inspection of phases II, III, and IV can be done from the detailed information contained in the lower panels of Figure 3. Phase II reveals a 100% NTCDI structure packed inside the wide terrace facet. Both III and IV phases show an approximate 75% BDG−25% NTCDI stoichiometry and random step edge decoration, although phase III belongs to a Au(677)-oriented

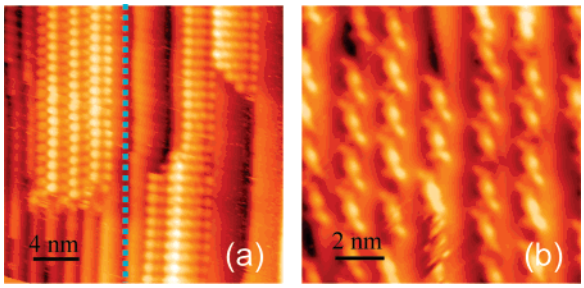

Figure 4. A 0.1 mL sample of (a) NTCDI and (b) BDG adsorbed on Au(455). NTCDI forms close-packed structures that accommodate on narrow and wide terraces, in contrast to BDG, which decorates step edges forming 1D H-bonded chains.

facet with a lower density of steps. The coexistence of pure-NTCDI, BDG-rich, and 50% phases indicates that the molecular recognition process is subject to limiting kinetics and/or new thermodynamics in stepped surfaces. Reduced diffusion across step edges might indeed play a role. However, it cannot be improved, since the postannealing treatment is in the limit of re-evaporation (especially, BDG). Reduced kinetics across the steps could explain the presence of a frustrated phase I characterized by a different stoichiometry, namely, the step-decorated BDG-rich III and IV phases in Figure 3c,d, respectively. However, the same phases with similar proportions segregate by direct coevaporation or sequential adsorption, with either molecule being evaporated first, and this rather points toward energy constraints, that is, competing driving forces.

In Figure 3, phases III and IV with large BDG concentration are step-decorated structures, in contrast to phase II, which is a terrace-filled NTCDI assembly. Such features actually reflect the distinct trend of NTCDI and BDG to aggregate or decorate steps, respectively, which is proved in Figure 4a,b. These panels respectively show the characteristic topography obtained after a 0.1 mL deposition of NTCDI and BDG on the vicinal Au(455) surface. To allow a direct comparison, for NTCDI the STM is focused on the boundary region between the narrow and wide terrace facets in Figure 4a (left and right from the blue dashed line, respectively). In both we observe packed, elongated NTCDI patches extending across monatomic steps and forming an oblique lattice inside terraces similar to the one shown in Figure 2b. It appears that surface steps are only forcing the elongated shape of the NTCDI aggregates. Moreover, we have not found any sign of NTCDI chaining on terraces or at step edges. For BDG, the hierarchy of driving forces is reversed, as shown in Figure 4b. It shows the STM image taken from BDG evaporated on a narrow terrace of Au(455). Similar images are obtained from wide terraces, that is, both wide and narrow terraces exhibit step decoration, with the BDG molecule axis being tilted by ~15° with respect to the step edge. That is needed to form a single BDG chain with a relatively strong double HNH···N bonding, as depicted in the bottom panel of Figure 2a.

Both the BDG tendency to decorate steps and the NTCDI trend to aggregate can force local 50% deviations in the stoichiometry of the mixture, as observed in phases II, III, and IV of Figure 3. Binary structures are not observed within narrow terraces, which only exhibit decorated steps and incomplete terrace filling. This strongly suggests terrace size restrictions on the BDG/NTCDI heterogeneous, molecular recognition assembly, such that only the BDG-rich IV phase would be allowed in narrow terraces. The excess of NTCDI is then forced to migrate and aggregate inside wide terraces. However, the presence of BDG-rich step-decorating phase III on wide terraces close to the NTCDI-rich aggregates of phase II also suggests that NTCDI clusters act as sinks for NTCDI molecules, thereby leading to the segregation of phase III. In such cases, kinetic parameters (annealing and molecule adsorption sequence) might result in a pure phase I structure, although this has not been achieved.

In summary, we prove that the coadsorption of linear, planar molecules with complementary end-groups give rise to supramolecular binary structures with strong uniaxial anisotropy. Au(111) vicinal surfaces are helpful to achieve single domains oriented along step edges. However, our experiments indicate that steps introduce a distinct hierarchy of driving forces for each molecule, leading to a multiple phase segregation. As a consequence, the presence of the ideal heterogeneous structure appears to be limited to surfaces with relatively wide terraces. Further experiments using single-phase vicinals with large terraces are encouraged.

Acknowledgment. We want to thank J. Cordón and F. Schiller for helping in the STM experiments and the data analysis, and A. P. Seitsonen and R. Fasel for very helpful discussions. This work was financed as part of the European Science Foundation EUROCORES Programme SONS (MAT2002−11975-E,) within the sixth European Community framework programme. Financial support from Eusko Jaurlaritza (Nanotron Project), Euskal Herriko Unibertsitatea, the Spanish Ministerio de Educacion y Ciencia (MEC), and the EU Network of Excellence NANOQUANTA (Grant No. NMP4-CT-2004-500198) is gratefully acknowledged. The SGI/IZO-SGIker UPV/EHU (supported by Fondo Social Europeo and MEC) is also acknowledged for its generous allocation of computational resources.

Supporting Information Available: Details about the chemical synthesis and characterization of BDG. This material is available free of charge via the Internet at http://pubs.acs.org.

References and Notes

(1) For a general introduction, see Service, R. F.; Szuromi, P.; Uppenbrink, J. *Science* **2002**, *295*, 2395−2491.

(2) Xu, S.; Dong, M.; Rauls, E.; Otero, R.; Linderoth, T. R.; Besenbacher, F. *Nano Lett.* **2006**, *6*, 1434−1438.

(3) Theobald, J. A.; Oxtoby, N. S.; Phillips, M. A.; Champness, N. R.; Beton, P. H. *Nature* **2003**, *424*, 1029−1031.

(4) Perdigão, L. M. A.; Perkins, E. W.; Ma, J.; Staniec, P. A.; Rogers, B. L.; Champness, N. R.; Beton, P. H. *J. Phys. Chem. B* **2006**, *110*, 12539−12542.

(5) Clair, S.; Pons, S.; Brune, H.; Kern, K.; Barth, J. V. *Angew. Chem., Int. Ed.* **2005**, *44*, 7294−7297.

(6) Repain, V.; Baudot, G.; Ellmer, H.; Rousset, S. *Europhys. Lett.* **2002**, *58*, 730−736.

(7) Kuntze, J.; Mugarza, A.; Ortega, J. E. *Appl. Phys. Lett.* **2002**, *81*, 2463−2465.

(8) Rousset, S.; Pourmir, F.; Berroir, J. M.; Klein, J.; Lecoeur, J.; Hecquet, P.; Salanon, B. *Surf. Sci.* **1999**, *422*, 33−41.

(9) Frisch, M. J.; Trucks, G. W.; Schlegel, H. B.; Scuseria, G. E.; Robb, M. A.; Cheeseman, J. R.; Zakrzewski, V. G.; Montgomery, Jr., J. A.; Stratmann, R. E.; Burant, J. C.; Dapprich, S.; Millam, J. M.; Daniels, A. D.; Kudin, K. N.; Strain, M. C.; Farkas, O.; Tomasi, J.; Barone, V.; Cossi, M.; Cammi, R.; Mennucci, B.; Pomelli, C.; Adamo, C.; Clifford, S.; Ochterski, J.; Petersson, G. A.; Ayala, P. Y.; Cui, Q.; Morokuma, K.; Salvador, P.; Dannenberg, J. J.; Malick, D. K.; Rabuck, A. D.; Raghavachari, K.; Foresman, J. B.; Cioslowski, J.; Ortiz, J. V.; Baboul, A. G.; Stefanov, B. B.; Liu, G.; Liashenko, A.; Piskorz, P.; Komaromi, I.; Gomperts, R.; Martin, R. L.; Fox, D. J.; Keith, T.; Al-Laham, M. A.; Peng, C. Y.; Nanayakkara, A.; Challacombe, M.; Gill, P. M. W.; Johnson, B.; Chen, W.; Wong, M. W.; Andres, J. L.; Gonzalez, C.; Head-Gordon, M.; Replogle, E. S.; Pople, J. A. *Gaussian 98*, revision A.11.3; Gaussian Inc.: Pittsburgh, PA, 2002.

(10) Frisch, M. J.; Trucks, G. W.; Schlegel, H. B.; Scuseria, G. E.; Robb, M. A.; Cheeseman, J. R.; Montgomery, Jr., J. A.; Vreven, T.; Kudin, K.

N.; Burant, J. C.; Millam, J. M.; Iyengar, S. S.; Tomasi, J.; Barone, V.; Mennucci, B.; Cossi, M.; Scalmani, G.; Rega, N.; Petersson, G. A.; Nakatsuji, H.; Hada, M.; Ehara, M.; Toyota, K.; Fukuda, R.; Hasegawa, J.; Ishida, M.; Nakajima, T.; Honda, Y.; Kitao, O.; Nakai, H.; Klene, M.; Li, X.; Knox, J. E.; Hratchian, H. P.; Cross, J. B.; Bakken, V.; Adamo, C.; Jaramillo, J.; Gomperts, R.; Stratmann, R. E.; Yazyev, O.; Austin, A. J.; Cammi, R.; Pomelli, C.; Ochterski, J. W.; Ayala, P. Y.; Morokuma, K.; Voth, G. A.; Salvador, P.; Dannenberg, J. J.; Zakrzewski, V. G.; Dapprich, S.; Daniels, A. D.; Strain, M. C.; Farkas, O.; Malick, D. K.; Rabuck, A. D.; Raghavachari, K.; Foresman, J. B.; Ortiz, J. V.; Cui, Q.; Baboul, A. G.; Clifford, S.; Cioslowski, J.; Stefanov, B. B.; Liu, G.; Liashenko, A.; Piskorz, P.; Komaromi, I.; Martin, R. L.; Fox, D. J.; Keith, T.; Al-Laham, M. A.; Peng, C. Y.; Nanayakkara, A.; Challacombe, M.; Gill, P. M. W.; Johnson, B.; Chen, W.; Wong, M. W.; Gonzalez, C.; Pople, J. A. *Gaussian 03*, revision C.02; Gaussian Inc.: Wallingdorf, CT, 2004.

(11) Tersoff, J. R.; Hamann, D. R. *Phys. Rev. B* **1985**, *46*, 6671−6687.

(12) Kresse, G.; Hafner, J. *Phys. Rev. B* **1994**, *49*, 14251−14269.

(13) Blochl, P. E. *Phys. Rev. B* **1994**, *50*, 17953−17979.

(14) Perdew, J. P.; Chevary, J. A.; Vosko, S. H.; Jackson, K. A.; Pederson, M. R.; Singh, D. J.; Fiolhais, C. *Phys. Rev. B* **1992**, *46*, 6671−6687.

(15) Rurali, R.; Lorente, N.; Ordejon, P. *Phys. Rev. Lett.* **2005**, *95*, 209601−1.

(16) Ruiz-Osés, M.; González-LaKunza, N.; Silanes, I.; Arnau, A.; Gourdon, A.; Ortega, J. E. Unpublished work, 2006.

(17) Keeling, D. L.; Oxtoby, N. S.; Wilson, C.; Humphry, M. J.; Champness, N. R.; Beton, P. H. *Nano Lett.* **2003**, *3*, 9−12.

(18) Note the difference from PTCDA/TBA binary chains (see Ma, J.; Rogers, B. L.; Humphry, M. J.; Ring, D. J.; Goretzki, G.; Champness, N. R.; Beton, P. H. *J. Phys. Chem. B* **2006**, *110*, 12207−12210), where strong interaction with the substrate (registry and orientation) prevents lateral interactions and 2D packing of chains.

(19) The two characteristic terrace sizes on molecule-covered surfaces slightly differ from the bare crystal surface, especially the narrow-terrace, (233)-oriented facet, which switches to an ∼(344) orientation. This indicates a minor reorganization of the substrate upon molecule adsorption.